UCRL-91484
PREPRINT

MODELING SHORT PULSE DURATION SHOCK INITIATION OF SOLID EXPLOSIVES

C. M. Tarver
J. O. Hallquist
L. M. Erickson

For submittal to: 8th Symposium (International)
on Detonation, Albuquerque, NM July 15-19, 1985

June 27, 1985

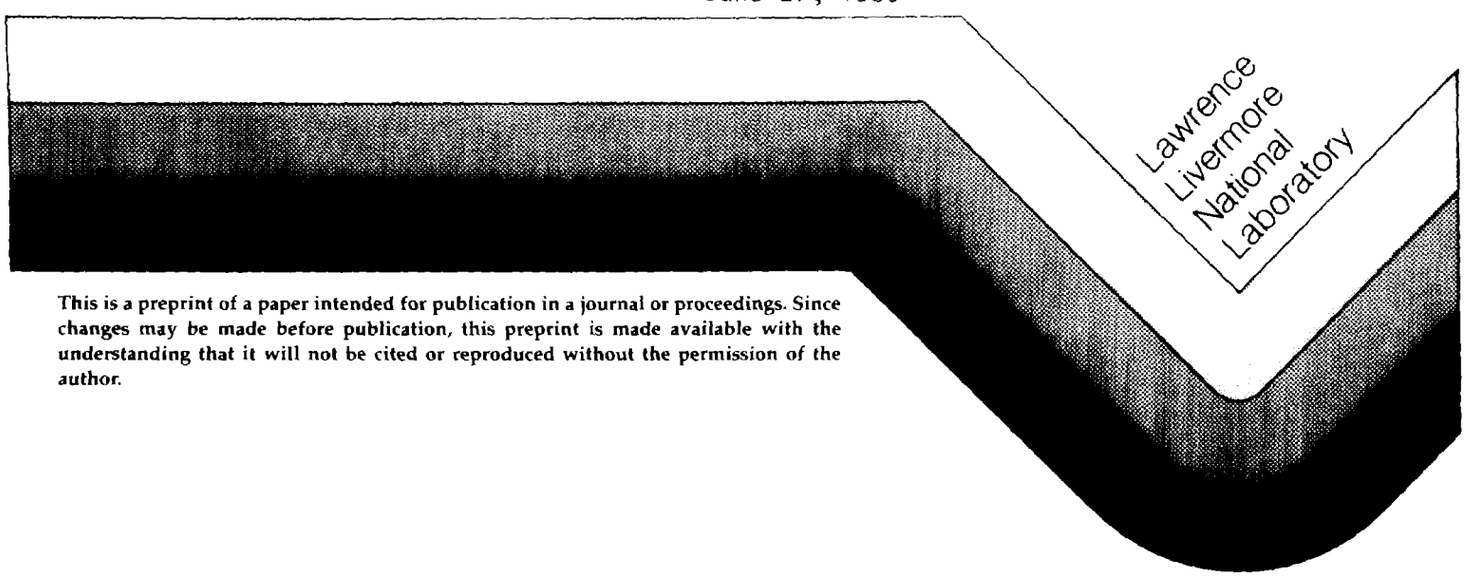

MODELING SHORT PULSE DURATION SHOCK INITIATION OF SOLID EXPLOSIVES

C. M. Tarver, J. O. Hallquist and L. M. Erickson
Lawrence Livermore National Laboratory
University of California
Livermore, California

The chemical reaction rate law in the ignition and growth model of shock initiation and detonation of solid explosives is modified so that the model can accurately simulate short pulse duration shock initiation. The reaction rate law contains three terms to model the ignition of hot spots by shock compression, the slow growth of reaction from these isolated hot spots, and the rapid completion of reaction as the hot spots coalesce. Comparisons for PBX 9404 between calculated and experimental records are presented for the electric gun mylar flyer plate system, the minimum priming charge test, embedded manganin pressure and particle velocity gauges, and VISAR particle velocity measurements for a wide variety of input pressures, rise times and pulse durations. The ignition and growth model is now a fully developed phenomenological tool that can be applied with confidence to almost any hazard, vulnerability or explosive performance problem.

INTRODUCTION

As an integral part of our High Explosives Research Program, the phenomenological ignition and growth computer model of shock initiation and detonation wave propagation has been developed to simulate the available experimental data and then to predict the hazard, vulnerability, and performance of solid explosives to various stimuli in complex geometries. The original one-dimensional ignition and growth model[1] successfully calculated a great deal of experimental data on several explosives including: embedded manganin pressure gauge and particle velocity gauge data, VISAR data, run distance to detonation versus initial shock pressure data, and quantitative failure initiation initiation data. After more experimental data was obtained and the model implemented in the two-and three-dimensional versions of the Lagrangian DYNA code[2], the ignition and growth model was modified and successfully applied to many one-, two- and three- dimensional initiation and detonation wave propagation problems in explosives and propellants[3-10]. In general, this concept of dividing the chemical reaction rate into two terms to describe the ignition of reaction by shock compression in localized hot spots and the subsequent growth of these hot spots to consume the explosive charge has proved sufficient for modeling sustained pulse shock initiation and detonation wave reaction zones. However, as noted in the original paper[1], detailed quantitative modeling of embedded gauge or VISAR data from short pulse duration shock initiation experiments was not possible unless the coefficient for the growth of reaction was increased by a factor of two or three. Although such a relatively simple phenomenological model can not be expected to perfectly simulate every shock initiation and detonation experiment, it is essential that the ignition and growth model accurately model initiation caused by a wide variety of input pressures, rise times and pulse durations. This paper describes the modifications to the chemical reaction rate law that were made to meet this requirement and the parameters generated for the solid explosives PBX 9404 (HMX-based) and LX-17 (TATB-based). This paper also contains several examples of the agreement between the calculations and recent experimental data from several laboratories on PBX 9404. Examples of modeling short pulse duration shock initiation of LX-17, shock initiation of a cast explosive, detonation wave propagation and metal acceleration, and supra-compression experiments with the current ignition and growth model are contained in four other papers presented at this Symposium[11-14].

THREE TERM REACTION RATE MODEL

During a review of embedded gauge data of Lagrange Analysis of such data[15] and of very high shock pressure, very short shock pulse duration initiation data, it became apparent that shock initiation of heterogeneous solid explosives must be modeled as at least a three

*Work performed under the auspices of the U.S. Department of Energy by the Lawrence Livermore National Laboratory under contract No. W-7405-ENG-48.

step process. The first step is obviously the formation of hot spots created by various mechanisms (void closure, viscous heating, shear banding, etc.) during shock compression and the subsequent ignition (or failure to ignite due to heat conduction losses) of these heated regions. At relatively low input shock pressures, the ignition of a fraction of the explosive on the order of the original void fraction of the charge is sufficient to calculate initiation/failure data and the increase in shock front pressure at increasing depths in embedded gauge experiments[1]. However, when modeling high input pressure, short pulse duration experiments, such as the minimum priming charge test[16] and initiation by thin mylar flyer plates in the electric gun[17], a larger fraction of the explosive must be rapidly ignited, especially with pressure dependent reaction growth rates. Therefore the main change in the ignition term of the reaction rate law was to increase the dependence of the amount of explosive ignited on the degree of shock compression, thereby igniting much more explosive at high pressures approaching detonation pressures and much less explosive at low input pressures of a few kilobars.

The second step in the process is assumed to be a relatively slow growth of reaction in inward and/or outward "burning" of the isolated hot spots. Although this analogy with deflagration processes may not be strictly appropriate under all shock initiation conditions, embedded gauge and VISAR experiments definitely show regions of relatively slow pressure and particle velocity increases behind the shock front. Modeling this portion of the reactive flow as a pressure dependent burn with an exponent near unity, as measured in deflagration experiments[18], readily matches sustained and short duration shock pulse data. In their Lagrange gauge and modeling work, Wackerle and Anderson[19] found that a simple spherical inward grain burning model yielded a better correlation with experimental data than a simple spherical outward hole burning model. Obviously the real situation of reacting hot spots is a much more complex geometry, but a spherical inward grain burning form is used along with a pressure exponent of one in the second or slow growth term of the reaction rate law in this paper.

The third step in the shock initiation process is a rapid completion of the reaction as the reacting hot spots begin to coalesce. Fast decomposition of the remaining pockets of unreacted explosive causes the rapid transition to detonation observed in wedge test run distance to detonation experiments[20]. If each hot spot is taken to be a sphere at the center of a cube, then, when the diameter of the sphere equals the length of a side of cube, the ratio of volume of the sphere to the volume of the cube is $\pi/6$ or 0.52. Therefore these idealized "spherical hot spots in a box" would begin to coalesce when the explosive is approximately half-reacted. Even for a relatively low input pressure of 2 GPa, the pressure exceeds 10 GPa when the explosive is half-reacted, and all conceivable reactive surface area generation mechanisms will be rapidly occurring. This rapid completion of reaction has been modeled in two ways: as an Arrhenius rate law with a realistic activation energy and realistic assumptions about the temperature of the unreacted explosive or as a pressure dependent growth rate with an exponent of two or three to match run distance to detonation data and to yield the correct reaction zone width for self-sustaining detonation. In this phenomenological model, the pressure dependent form is used to represent the third part of the initiation model: the rapid completion of reaction as the turnover to detonation occurs.

Therefore the form of the chemical reaction rate equation in the three term ignition and growth model is:

$$\partial F/\partial t = I(1-F)^{b}(\rho/\rho_o - 1 - a)^{x} + G_1(1-F)^{c}F^{d}p^{y} + G_2(1-F)^{e}F^{g}p^{Z} \qquad (1)$$

where F is the fraction of the explosive that has reacted, t is time, ρ_o is the initial density of the explosive, p is pressure in megabars, and I, G_1, G_2, a, b, c, d, e, g, x, y, and Z are constants. The parameter a is a critical compression that is used to prohibit ignition until a certain degree of compression (or a certain input pressure) has been reached. In most cases, the parameter y in the first growth rate term is set equal to one to represent a deflagration process. The parameters b and c on the $(1-F)$ terms in the ignition and first growth terms are set equal to 2/3 to represent inward spherical grain burning. The parameters I and x control the amount of ignition as a function of shock strength and duration, G_1 and d control the early growth of reaction following ignition, and G_2 and Z determine the high pressure reaction rates. Maximum and minimum values of F have been added to the reaction rate computations so that each of the three rates can be turned off (or turned on) at appropriate values. The ignition rate is set equal to zero when F exceeds the parameter Figmax. The first growth rate is set equal to zero when F exceeds the parameter F_{G1max}. The second growth rate is zero when F is less than F_{G2min}.

The values of all the parameters used for PBX 9404 and LX-17 are listed in Table 1. The unreacted and reaction product equations of state for PBX 9404 and LX-17 remain the same as those given by Tarver and Hallquist[3]. The mixture rules and methods of calculation remain the same as in the original description[1]. The results of using this three term rate law to simulate many experiments on PBX 9404 are described in the next section. Similar

calculations of the available LX-17 experimental data are contained in a companion paper[11].

TABLE 1 CHEMICAL REACTION RATE PARAMETERS FOR PBX 9404 AND LX-17

Parameter (EQ.(1))	PBX 9404	LX-17
I (μsec^{-1})	7.43×10^{11}	4.0×10^{6}
b	0.667	0.667
a	0.0	0.22
x	20.0	7.0
G_1 ($Mbars^{-Y}$ μsec^{-1})	3.1	0.6
c	0.667	0.667
d	0.111	0.111
y	1.0	1.0
G_2 ($Mbars^{-Z}$ μsec^{-1})	400.0	400.0
e	0.333	0.333
g	1.0	1.0
Z	2.0	3.0
Figmax	0.3	0.5
F_{G1max}	0.5	0.5
F_{G2min}	0.0	0.0

Comparison of Calculations and Experimental Results for PBX 9404

1. High Pressure, Short Pulse Duration Tests

A good, overall quantitative test of a reactive flow model is the one-dimensional initiation/failure data generated by accelerating various thicknesses of mylar by electrically exploded aluminum foils, as described by Weingart et.al[17]. The decay of the pressure behind the mylar foil depends on its acceleration history, the amount of electrical energy used, and the presence of remaining aluminum vapor. For conservative modeling, the mylar flying plates are assumed to be fully accelerated with no vaporized material still accelerating them. The experimental threshold velocities for six thicknesses of mylar ranging from 1.27-mm to 0.025-mm for shock initiation of 19-mm thick PBX 9404 charges are listed in Table 2, along with the calculated threshold velocities for comparison. The pressures produced by the thinnest flyers may approach the von Neumann spike pressure of the explosive and the shock pulse duration may be only a few nanoseconds, so very finely zoned calculations with 100 zones/mm in the explosive are necessary to accurately resolve these shock fronts. The agreement between the calculations and experiments is good at the higher pressures, where 20-30% of the explosive is ignited by the shock front, and at the lower pressures where a few tenths of a percent of the explosive is promptly ignited. At the two intermediate pressures the calculations predict higher threshold velocities than measured. However, in these experiments, considerable aluminum vapor is still accelerating the plates, and the pressure decay behind the flyer is not as steep as assumed in the calculations and more reaction can occur behind the main front, thus lowering the initiation threshold. Care must also be taken in defining detonation, because, in these experiments, a flash from $Al_2(SiF_6)_3$ coated on the rear face of explosive charge detects a shock wave pressure of approximately 20 GPa. The calculations show that it is possible with a high initial shock pressure to obtain a 20 GPa shock front emerging from the explosive rear boundary that is actually slowly failing or slowly building toward detonation. Considering these experimental uncertainties, which must be considered when calculating any experiment, the three term reaction rate model does a reasonably good job on the electric gun data.

TABLE 2 VELOCITY THRESHOLDS FOR MYLAR FLYER INITIATION OF PBX 9404 IN THE ELECTRIC GUN

Mylar Flyer Thickness (mm)	Experimental Velocity Threshold (Km/s)	Calculated Velocity Threshold (Km/s)
1.27	1.1 ± 0.2	0.95 ± 0.05
0.508	1.4 ± 0.2	1.30 ± 0.10
0.254	1.9 ± 0.2	2.55 ± 0.05
0.127	2.6 ± 0.2	2.95 ± 0.05
0.051	3.3 ± 0.3	3.55 ± 0.05
0.025	4.2 ± 0.3	3.95 ± 0.05

2. Minimum Priming Charge Test

A tougher high pressure, short shock pulse duration test for this model is the one-dimensional, spherically divergent initiation of PBX 9404 by PETN-based EXTEX in the minimum priming charge test[16]. Hemispheres of EXTEX of varying radii are centrally detonated and produce 20.5 GPa peak pressure pulses with different Taylor waves in the acceptor samples. The critical radius for initiation of detonation is then determined. For PBX 9404 the 50% point for shock initiation is 0.195 cm of EXTEX. In modeling this test, a spherically divergent Chapman Jouguet detonation wave in EXTEX (ρ_o= 1.54g/cm^3, D = 7.35 mm/ μs, P_{CJ} = 20.5 GPa, JWL coefficients : A = 5.39165 Mbars, B = 0.0334709 Mbars, R_1 = 4.6, R_2 = 1.1, ω= 0.4, E_o = 0.066 Mbars-cc/cc) is assumed to impact finely zoned (100 zones/mm) PBX 9404. Figure 1 shows calculated pressure profiles at various distances into PBX 9404 for a 0.19 cm radius EXTEX charge which illustrate the failure to shock initiate the PBX 9404. Figure 2 shows similar profiles for a 0.20 cm radius EXTEX charge which illustrate the successful initiation of spherically divergent detonation in the PBX 9404. The reactive flow model clearly has the correct pressure, time duration and geometric dependences for successful calculations of this test.

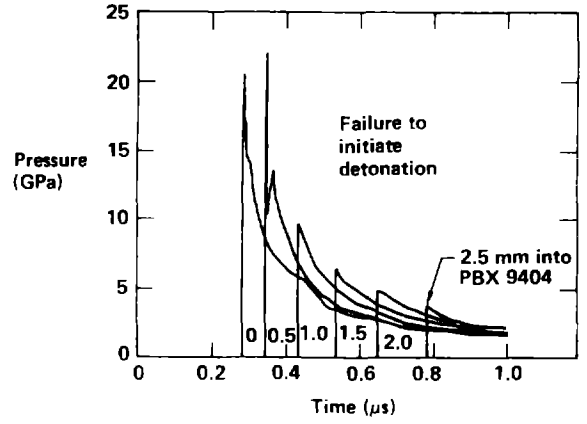

Fig. 1. Calculated pressure histories in PBX 9404 for a 0.2 cm radius minimum priming charge.

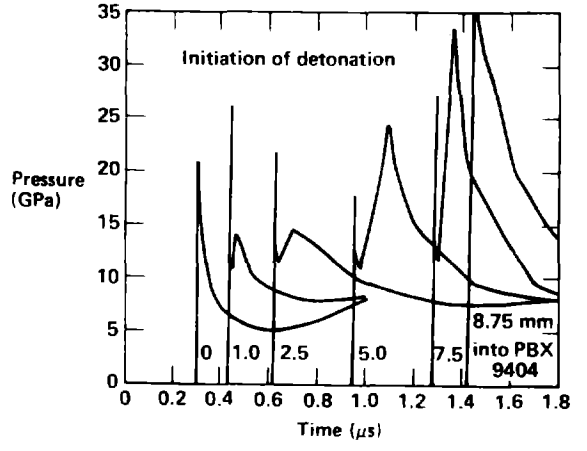

Fig. 2. Calculated pressure histories in PBX 9404 for a 0.2 cm radius minimum priming charge.

3. Lower Pressure Sustained and Short Duration Embedded Gauge Experiments

Two classical sets of embedded gauge experiments on PBX 9404 have been done in the 2.5-3.5 GPa initial shock pressure range to demonstrate the differences in the growth to detonation for sustained short duration shock pulses. Wackerle et al.[21] placed one manganin pressure gauge in each sample and fired several PBX 9404 samples with gauges placed at different depths. The experimental records from these experiments are superimposed in Figures 3 and 4 for a 3 GPa sustained shock and a 3 GPa, 0.33 μs shock pulse, respectively. The calculations must be done exactly as were the experiments, since the finite thickness of a manganin gauge (typically 1 mil of manganin foil sandwiched between two 5 to 10 mil thick layers of teflon, kapton, mylar or mica insulation) does perturb the reactive flow. This is even more important in multiple manganin gauge experiments[1, 3, 11] in which several gauges are placed in the same explosive sample. Figures 3 and 4 also contain the calculated pressure histories at the various gauge positions. The calculated pressures agree well with the gauge records up to the pressures at which these gauges failed. The calculated run distances to detonation of 9.5-mm and 15-mm for the sustained shock and the 0.33 μs pulse, respectively, agree with the experimental values of 9.5-mm and 14.5-mm. At the 1-mm and 3-mm gauge positions of Figure 4, the calculated shock front amplitude and initial rarefaction agree with the gauge records but subsequent pressures are lower than the gauge records indicate. It is difficult to determine whether this difference is totally due to the reaction rate law or whether part of the difference is due to the current lack of knowledge of the reaction products equation of state and of the accuracy of the mixture assumptions in this pressure and temperature regime. Since the ignition and growth model must also describe detonation and its metal acceleration ability correctly, it uses JWL equation of state for the reaction products measured by expansion in detonation experiments. There is no guarantee that this equation of state accurately predicts the states of products generated in low pressure shock initiation experiments, but this is the assumption that must be made in this general purpose model. It should be mentioned that manganin pressure gauges have undergone further development and currently can record the entire reactive flow process without failing in both shock initiation and full detonation[3, 7, 11].

In the other set of embedded gauge experiments, multiple particle velocity gauges measured the growth to detonation caused by a sustained 3 GPa shock pressure in Figure 5, a 2.5 GPa, 1 μs shock pulse from a dynasil flyer in Figure 6, and a 2.2 GPa, 1 μs shock pulse from a Kel-F flyer in Figure 7. These embedded particle velocity gauges have the advantage that they are much thinner than manganin gauges (typically 1 mil of aluminum with 1 mil of teflon on each side), but the disadvantage that non-metallic flyer plates must be used. Thus not all pressure regimes are easily accessible and the non-metallic materials have equations of state that are not as well understood as those of metals. These experimental details are modeled as completely as possible in Figures 5, 6, and 7. The agreement between the calculated and experimental shock front and subsequent growth in the sustained shock experiment in Figure 5 is quite close. In the dynasil flyer experiment shown in Figure 6, the calculated shock front particle velocity is high at the 14-mm gauge position and the calculated peak particle velocity occurs early, thus implying a slightly early transition to detonation. By the 22-mm gauge position, however, both the calculation and the gauge record indicate that

detonation has occurred. It should be mentioned that the particle gauges used in Figs. 5 and 6 recorded incorrect (low) velocities only at full detonation. This problem was solved by teflon insulation, as demonstrated by published gauge records in full detonation[7, 9]. In the Kel-F flyer experiment shown in Fig. 7, the reactive flow is building toward detonation but does not quite make the transition in 22-mm sample of PBX 9404. The calculations predict slightly high particle velocities, particularly at the 14-mm position, and a transition to detonation in less than 22-mm. Therefore it appears that the model predicts slightly too much ignition and early growth at these low input shock pressures, perhaps due to the fact that the unreacted equation of state does not fully describe the dissipative processes first measured by Kennedy and Nunziato[22] in PBX 9404 below 3 GPa and also observed in Lagrange analysis of embedded gauge records[15]. Mechanical dissipation processes or endothermic chemical reactions can be added to the model when they are identified and measured quantitatively.

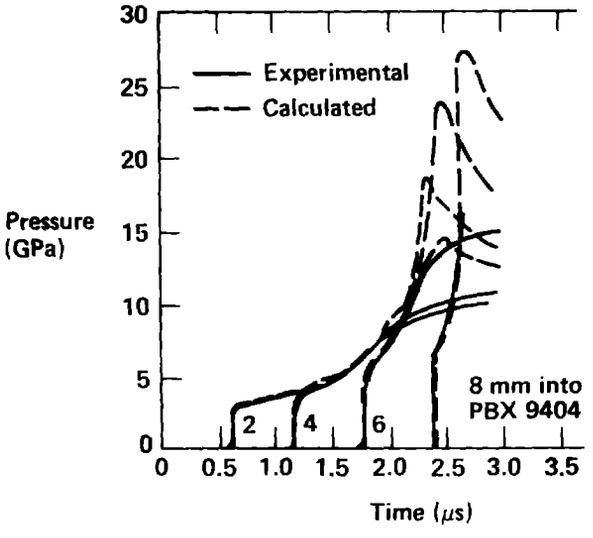

Fig. 3. Pressure Histories for a 3 GPa sustained shock wave in PBX 9404

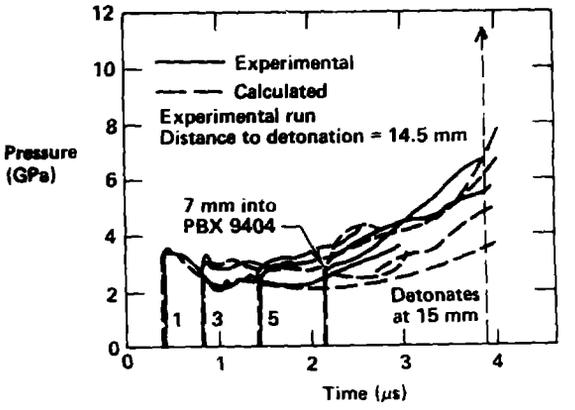

Fig. 4. Pressure histories for a 3 GPa, 0.33μs shock pulse into PBX 9404

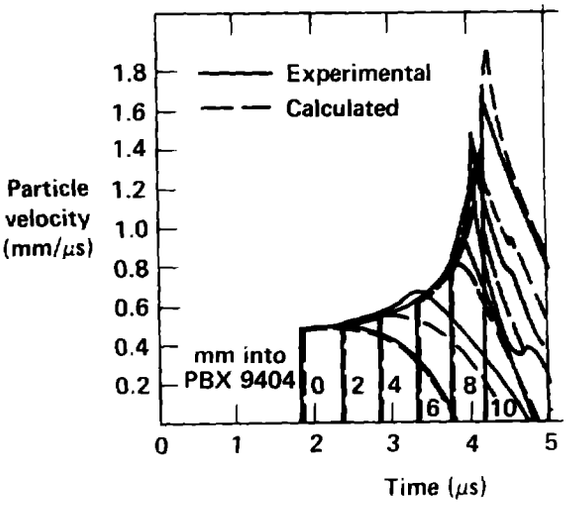

Fig. 5. Particle velocity histories for a sustained 3.5 GPa shock wave into PBX 9404

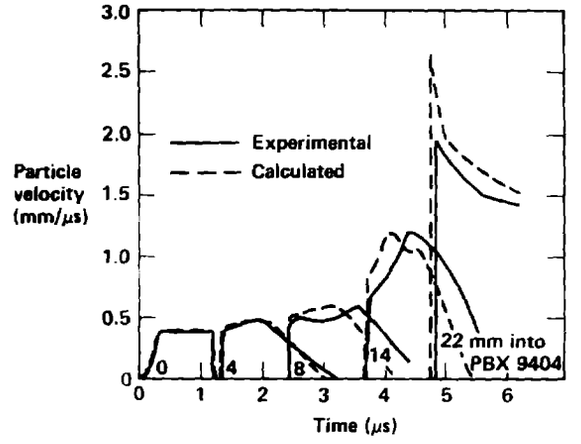

Fig. 6. Particle velocity histories for a dynasil flyer plate short duration shock pulse in PBX 9404

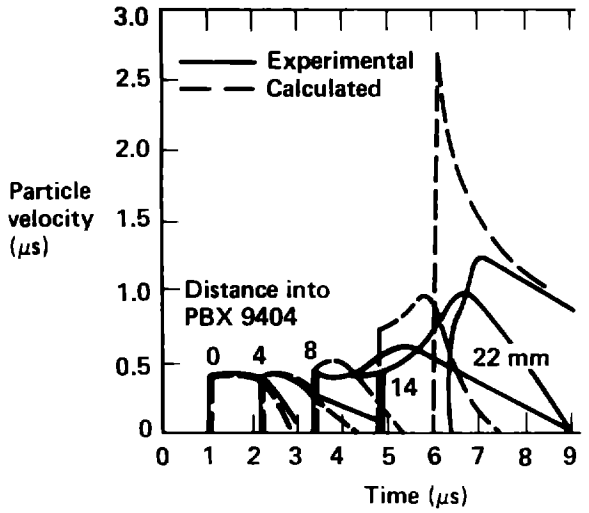

Fig. 7. Particle velocity histories in PBX 9404 for a Kel-F flyer plate short duration shock pulse.

4. VISAR Records of Various Initiation Experiments on PBX 9404

In an imaginative series of experiments on PBX 9404, Setchell[23-25] measured the growth of reaction in PBX 9404 subjected to several types of input stresses using a VISAR particle velocity measurement technique. Setchell used various combinations of flyer plate and buffer materials in front of the explosive samples to produce short duration shock pulses with different unloading histories, ramp waves, two step shocks, ramp/shock loading, and low amplitude precursor/shock loading. These experiments produced sets of particle velocity histories for various thicknesses of PBX 9404 that represent excellent tests for computer modeling. Besides testing the reactive flow model, these experiments also test the complex material models for the flyer plate, buffer and window materials: fused silica, sapphire, copper, pyroceram, 6061-T6 aluminum, tungsten, and even the carbon foam backing on the impactors. The VISAR records are very accurate measurements of the ignition and early slow growth of reaction, but are limited to stresses below 7.5 GPa in PBX 9404 because of a phase transition at 9.4 GPa in the fused silica window behind the explosive sample. To test the effect of different unloading histories on the growth of reaction in a short duration shock pulse experiment, Setchell[23] impacted PBX 9404 with fused silica (fast unloading) and sapphire (slow unloading) to produce 3.2 GPa, 0.37 μs initial shock pressures. The resulting particle velocity histories are shown in Figure 8 for 2, 4, 6 and 10mm of PBX 9404 impacted by fused silica and in Figure 9 for 2, 4, 6 and 8mm samples impacted by sapphire. The slower unloading properties of sapphire obviously allowed more reaction to occur and thus higher particle velocities were recorded. Figures 8 and 9 also contain the calculated particle velocity histories for each of the eight experiments. In the case of fused silica impact in Fig. 8, the initial shock pulse and unloading are well modeled since the 2-mm records agree closely. At greater depths, the calculated initial particle velocities are higher than measured, due to slightly too much ignition or a lack of dissipation processes, and the later portions of the calculated records are generally slightly lower than the measurements. The late time agreement in the 10-mm experiment is very good. In the case of sapphire impact in Fig. 9, much less shock front decay is observed and the calculated initial particle velocities are in better agreement. Again the calculated particle velocities are generally slightly lower than the experiments records, but the overall more rapid growth for sapphire impact is reproduced by the calculations shown in Fig. 9.

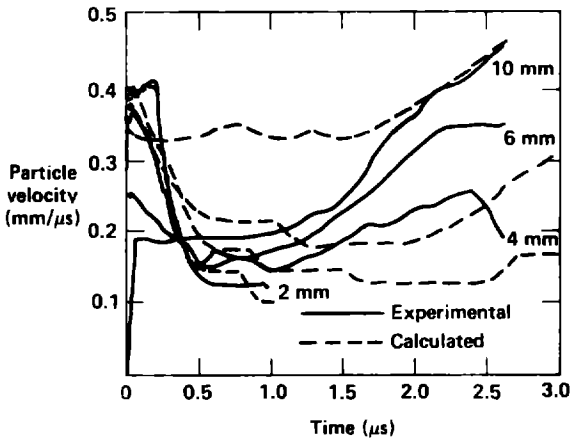

Fig. 8. Particle velocity histories in PBX 9404 for fused silica flyer plate experiments.

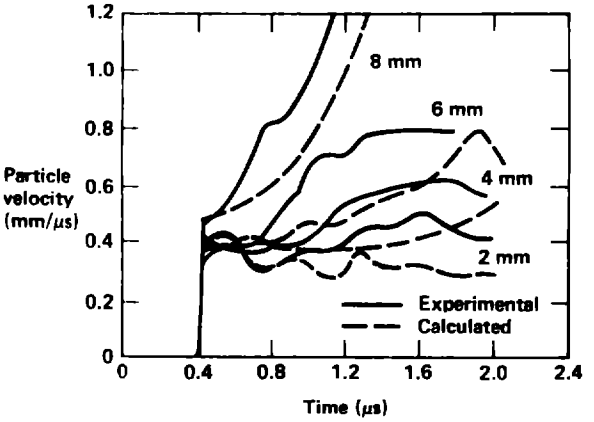

Fig. 9. Particle velocity histories in PBX 9404 for the sapphire flyer plate experiments.

The same relationship between experimental and calculated particle velocity histories is observed for Setchell's experiments in which 6061-T6 aluminum is placed in front of PBX 9404 producing a low amplitude precursor which precedes a 3.5 GPa shock[25]. The comparisons for 1.5, 4 and 6mm of PBX 9404 are shown in Figure 10. However, this relationship does not always hold, as shown in Figure 11, which contains comparisons at 2, 3, 4 and 5mm depths for the case of "ramp/shock" loading. A 2 GPa, 0.5 μs ramp receding a 5 GPa shock is produced by using a 19mm thick fused silica buffer ahead of the PBX 9404. In Fig. 11, the calculations lie slightly above the experimental records at 2, 3 and 4mm and slightly below at 5mm. For the case of a two step shock produced by a composite flyer plate of fused silica and tungsten (25), the calculations predict slightly higher particle velocities than measured at 2, 3 and 4mm of PBX 9404, as shown in Fig. 12.

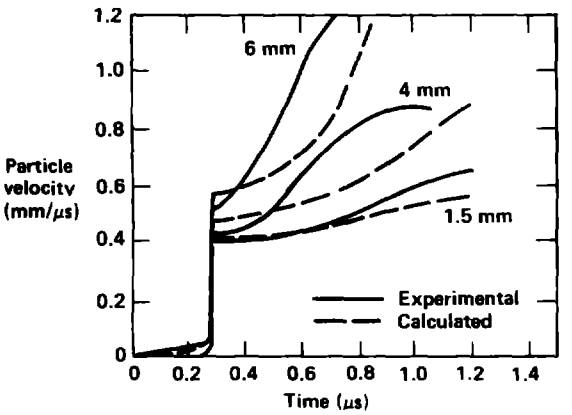

Fig. 10. Particle velocity histories in PBX 9404 for 3.5 GPa shocks preceded by low amplitude precursors.

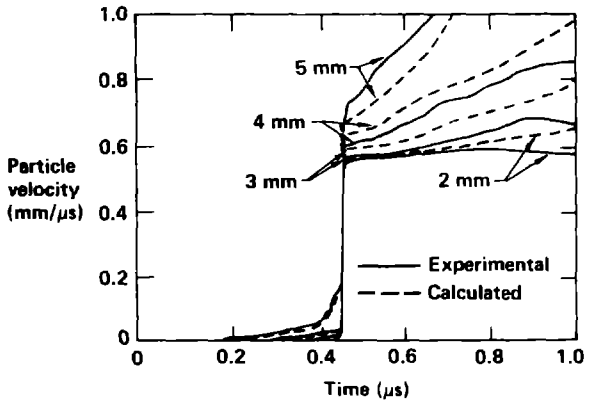

Fig. 11. Particle velocity histories in PBX 9404 for the ramp/shock experiments.

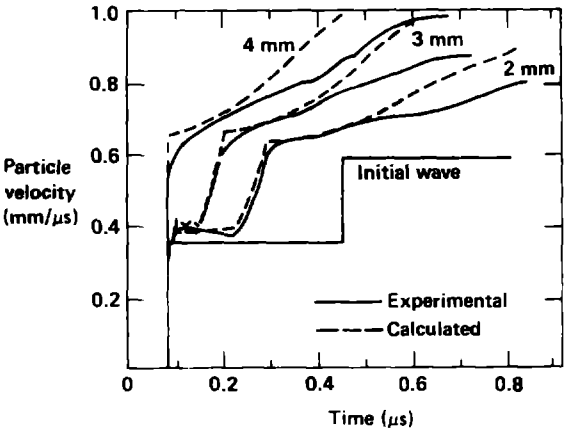

Fig. 12. Particle velocity histories in PBX 9404 for the two step shock loading experiments.

The final three comparisons with Setchell's data are shown in Figs. 13, 14 and 15 for the cases of slow rising (0.8 μs) ramp waves, faster rising (0.3 μs) ramp waves, and sharp shock loading to a final pressure of 5.1 GPa, respectively (24). The calculations accurately predict the initial ramp wave loadings in Figs. 13 and 14. In the slow ramp case in Fig. 13, the calculated particle velocities are low at 1.5 and 2-mm and then high at 3, 4 and 5mm. In the fast ramp and shock cases of Figs. 14 and 15, respectively, the calculated particle velocity histories are all slightly lower than the VISAR records.

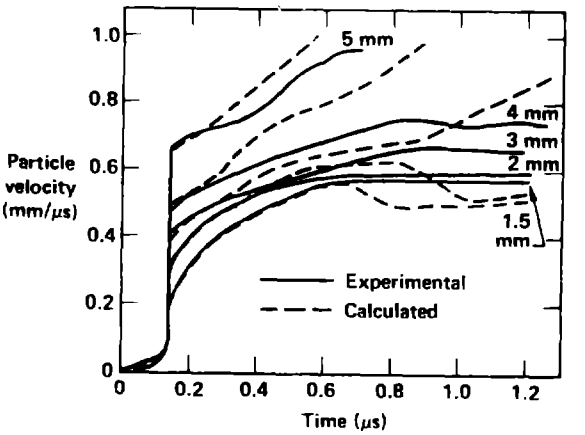

Fig. 13. Particle velocity histories in PBX 9404 for the slow ramp wave experiments.

The main result of these comparisons is that the three reaction rate law for PBX 9404 does a good overall job of describing initiation under a wide range of loading and unloading conditions. Further small modifications in the ignition and early growth rates, plus the inclusion of energy dissipation terms in the unreacted equation of state, would result in slightly improved agreement in various pressure and time regimes. However, the current agreement certainly demonstrates the soundness of this modeling approach.

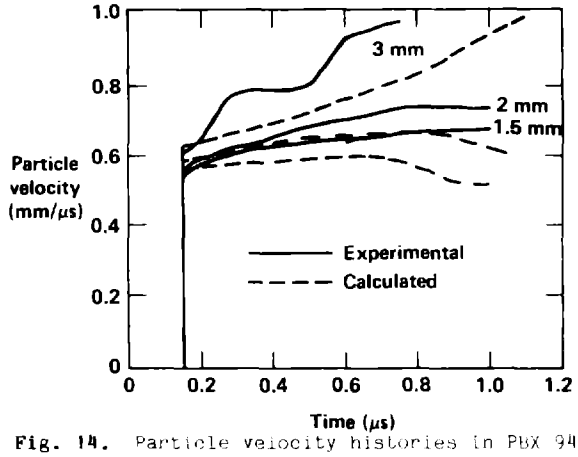

Fig. 14. Particle velocity histories in PBX 9404 for the fast ramp wave experiments.

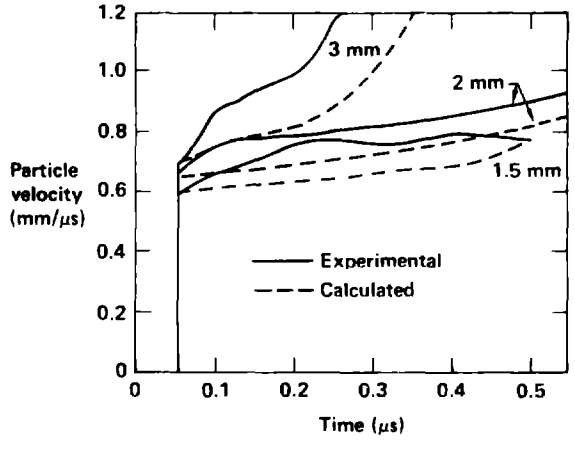

Fig. 15. Particle velocity histories in PBX 9404 for the 5.1 GPa sustained shock experiments.

One other interesting comparison between a embedded gauge experiment and a PBX 9404 reactive flow calculation is currently available. Many hazard and vulnerability scenarios for explosives involve two or more shocks separated in time by various unloading processes. In the experiment shown in Fig. 16, embedded particle velocity gauges at 0, 4, 7, 12 and 20mm depths measured the double shocks produced by the impact of a composite flyer consisting of two ceramic plates separated by low density carbon foam. The growth of reaction during the time between shocks and after the second shock produces a complex wave structure that is approaching the transition to detonation after 20mm of propagation. The calculated particle velocity histories are also shown in Fig. 16. The double shock structure is evident but the calculated particle velocities behind the first shock are low and the second shock arrivals are later in time than measured. This most likely results from an incomplete understanding of the equation of state of the ceramic flyer and buffer plate material and of the density and thickness of the compressible carbon foam when impact actually occurs. More experiments of this type should enable us to understand these materials and to "fine tune" the ignition and growth coefficients for reliable multiple shock scenario predictions.

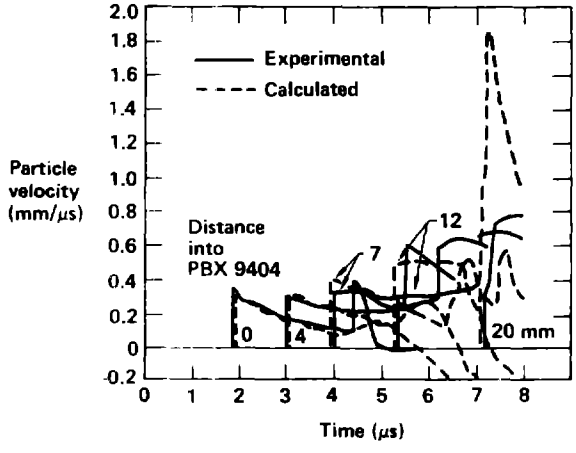

Fig. 16. Particle velocity histories in PBX 9404 for a double separated shock experiment.

CONCLUSIONS

The results presented in this paper show that the use of a three term chemical reaction rate equation in the phenomenological ignition and growth model yields good overall agreement with a large collection of shock initiation data on PBX 9404 from three laboratories. Therefore we now have a general purpose model that can be used with confidence to simulate most initiation scenarios. Obviously the coefficients in the model can be further modified to improve the agreement with existing and future data. As a by-product of this work, the consistent agreement of the calculations with the various experimental techniques (embedded manganin pressure gauges, embedded particle velocity gauges and VISAR) implies that the three techniques are all accurately recording the effects of the shock initiation process.

With the completion of the phenomenological model of shock initiation, the direction for future work is the development of more fundamental, microscopic models that describe actual ignition and growth processes. These models are needed to predict the effects of particle size and initial temperature on shock initiation. Our first step in this direction is the statistical hot spot model, which contains a critical hot spot size parameter and does accurately simulate particle size effects in TATB[26]. This model has recently been made entirely temperature dependent[27] and represents the starting point for the next generation of shock initiation models for solid explosives.

ACKNOWLEDGMENTS

The authors would like to thank all of the scientists that have taught us so much about reactive flow over the years especially: M. Cowperthwaite of SRI International; R. Setchell, J. Kennedy, J. Nunziato and P. Taylor of Sandia National Laboratory; J. Wackerle, M. Ginsberg, J. Vorthmann, W. Seitz, A. Anderson, P. Tang and C. Forest of Los Alamos National Laboratory; and all of our co-workers at Lawrence Livermore National Laboratory.

REFERENCES

1. E. L. Lee and C. M. Tarver, Phys. Fluids 23, 2362 (1980).

2. J. O. Hallquist, "User's Manual for DYNA2D", Lawrence Livermore National Laboratory Report UCID-18756 Rev. 2, January 1984.

3. C. M. Tarver and J. O. Hallquist, Seventh Symposium (International) on Detonation, Naval Surface Weapons Center NSWC MP-82-334, Annapolis, MD, 1981, p. 488.

4. B. Hayes and C. M. Tarver, ibid., p. 1029.

5. W. G. Von Holle and C. M. Tarver, ibid., p.993.

6. L. G. Green, E. James, E. L. Lee, E. S. Chambers, C. M. Tarver, C. Westmoreland, A. M. Weston and B. Brown, ibid., p. 256.

7. C. M. Tarver, N. L. Parker, H. G. Palmer, B. Hayes and L. M. Erickson, J. Energetic Materials 1, 213 (1983).

8. C. M. Tarver and P. A. Urtiew, Progress in Astronautics and Aeronautics 94, 369 (1983).

9. C. M. Tarver, L. M. Erickson and N. L. Parker, Shock Waves in Condensed Matter-1983 (J. R. Asay, R. A. Graham, G. K. Straub, eds.), North-Holland, Amsterdam, 1984, p. 609.

10. S. A. Sheffield, D. D. Bloomquist and C. M. Tarver, J. Chem. Phys.80, 3831 (1984).

11. K. Bahl, G. Bloom, L. Erickson, C. Tarver, W. Von Holle, R. Weingart, and R. Lee "Initiation Studies on LX-17", paper presented at this Symposium.

12. L. G. Green, E. L. Lee, A. C. Mitchell and C. M. Tarver, "The Supra-compression of LX-07 LX-17, PBX-9404, and RX-26-AF and the Equations of State of the Detonation Products", Lawrence Livermore National Lab, June 27, 1985, paper presented at this Symposium.

13. E. L. Lee, private communications, LLNL, 1985.

14. Moulard, H., Kury, J. K., Delclois, A., "The Effect of RDX Particle Size on the Shock Sensitivity of Cast PBX Formulations," UCRL 92473, paper presented at this Symposium.

15. G. L. Nutt and L. M. Erickson, J. Energetic Materials 2, 263 (1984).

16. C. A. Forest, "Numerical Modeling of the Minimum Priming Charge Test", Los Alamos National Laboratory Report LA-8075, February 1980.

17. R. C. Weingart, R. K. Jackson, C. A. Honodel and R. S. Lee, Propellants and Explosives 5, 154 (1980).

18. T. L. Boggs, C. F. Price, A. I. Atwood, D. E. Zurn, and R. L. Derr, Seventh Symposium (International) on Detonation, Naval Surface Weapons Center NSWC MP82-334, Annapolis, MD, 1981, p. 216.

19. J. Wackerle and A. B. Anderson, Shock Waves in Condensed Matter - 1983 (J. R. Asay, R. A. Graham, G. K. Straub, eds.), North-Holland, Amsterdam, 1984, p. 601.

20. J. B. Ramsay and A. Popolato, Fourth Symposium (International) on Detonation, Office of Naval Research ACR-126, White Oak, MD, 1965, p.233.

21. J. Wackerle, R. L. Rabie, M. J. Ginsberg, and A. B. Anderson, Symposium (International) on High Dynamic Pressures, Commissariat a l'Energie Atomique, Paris, 1978, p. 127.

22. J. E. Kennedy and J. W. Nunziato, J. Mech. Phys. Solids 24, 107 (1976).

23. R. E. Setchell, Seventh Symposium (International) on Detonation, Naval Surface Weapons Center NSWC MP82-334, Annapolis, MD, 1981, p. 857.

24. R. E. Setchell, Comb. Flame 43, 255 (1981).

25. R. E. Setchell, Comb. Flame 54, 171 (1983).

26. S. G. Cochran and C. M. Tarver, Shock Waves in Condensed Matter - 1983 (J. R. Asay, R. A. Graham, G. K. Straub, eds.), North-Holland, Amsterdam, 1984, p.593.

27. J. D. Immele, Private Communication, LLNL, 1985.